Regular Article

PHYSICAL CHEMISTRY RESEARCH
Published by the
Iranian Chemical Society
www.physchemres.org
info@physchemres.org

***Phys. Chem. Res.**, Vol. 1, No. 2, 117-125, December 2013.*

Computational Study of the Intramolecular Proton Transfer between 6-Hydroxypicolinic Acid Tautomeric Forms and Intermolecular Hydrogen Bonding in their Dimers

S.H. Kazemi, H. Eshtiagh-Hosseini, M. Izadyar and M. Mirzaei*

Department of Chemistry, Faculty of Science, Ferdowsi University of Mashhad, Mashhad 917751436, Iran

(Received 28 May 2013, Accepted 20 July 2013)

This paper is a density functional theory (DFT) calculation of intramolecular proton transfer (IPT) in 6-hydroxypicolinic acid (6HPA, 6-hydroxypyridine-2-carboxylic acid) tautomeric forms. The transition state for the enol-to-keto transition is reported in the gas phase and in four different solvents. The planar and non-planar dimer forms of 6HPA keto and enol, respectively, were also studied in the gas phase The IPT reactions and dimerization processes were studied at the B3LYP/6-31++G(d) level of the theory. The influence of the solvent on the tautomerization reaction of 6HPA was examined using the conductor-polarizable continuum model (CPCM). The IPT reaction in the gas phase is almost the same as in solution. The calculated dimerization energies show that the stability of 6HPA tautomer dimer structures is directly affected by the distance of intermolecular hydrogen bonding and electrostatic potential (ESP) value in the tautomer dimer.

Keywords: Intramolecular proton transfer (IPT), Intermolecular hydrogen bonding, 6-Hydroxypicolinic acid (6HPA), Electrostatic potential (ESP), Tautomerization

INTRODUCTION

Proton tautomerism is a general phenomenon in organic molecules and has a crucial role in many fields of acid-base chemical and biological dynamics caused by site specific interaction such as hydrogen bonding. In recent years, the important role of hydrogen bonds in physics, chemistry and biology has attracted more and more attention to the intramolecular proton transfer (IPT) along hydrogen bonding [1-19]. 6-Hydroxypicolinic acid (6HPA, 6-hydroxypyridine-2-carboxylic acid, $C_6H_5NO_3$) has several interesting characteristics: first, it is characterized by a enol-keto tautomerism [20-22]; second, it has a potential chelate with interesting possibilities, exhibiting either N,O-chelation (through the N atom and the carboxylate group, forming a five-membered chelate ring) or N,O,O-chelation (through the N atom and the carboxylate group, and further through the deprotonated hydroxy group as a bridging ligand), it is capable of coordinating to the various metal ions [21-29], and third, it is not only a potential proton acceptors but also proton donors depending on deprotonated groups [23,30]. 6HPA clearly indicates the enol-keto tautomerism of the CONH moiety, as shown in Fig. 1. Since the labile hydrogen atom of the OH group is close to the basic nitrogen atom, and the hydrogen can be easily transferred to it. The keto form is more preferable than the enol form. The latest study by Kukovec et al reports that 6HPA is planar and crystallize in keto form and stabilized in the solid state through a strong symmetric double hydrogen bond [22]. **Keto** tautomer is the minimum structure taking into account that its total electronic energy plus the zero point energy is lower than enol form in the gas phase. The carboxyl protons are involved in the intra and intermolecular hydrogen bonds (lone pairs of N atom of pyridine and O atom of carboxyl can be hydrogen bond acceptors). Therefore, 6HPA is a good model compound for intra and intermolecular proton transfer studies. In the present work, we have studied the IPT reaction between the

*Corresponding author. E-mail: mirzaeesh@um.ac.ir

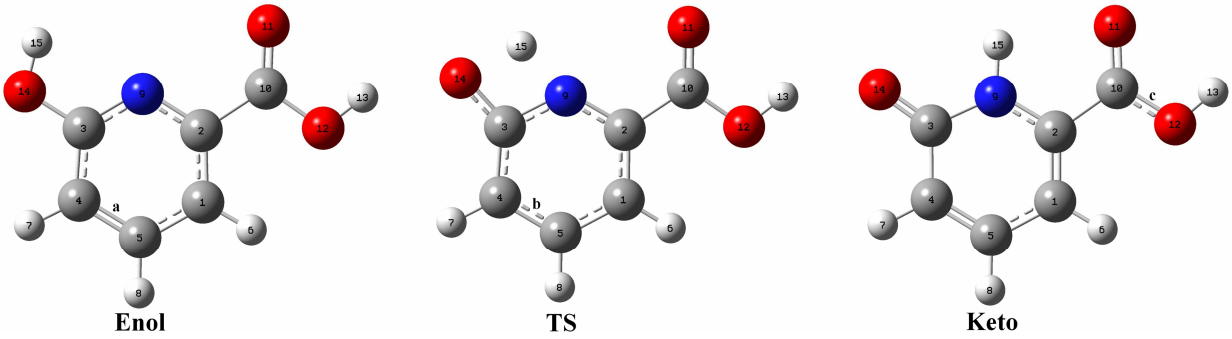

Fig 1. Optimized tautomer molecular structures of **Enol**, **Keto** and the transition state (**TS**). Carbon atoms are colored in gray, oxygen atoms in red, nitrogen atoms in blue, and hydrogen atoms in white. (a) The C4C5 bond is aromatic, in the gas phase. (b) The C4C5 bond is double, in the gas phase. (c) The C10O12 bond is single, in the gas phase.

Enol and **Keto** tautomers of 6HPA. In order to follow the atoms of 6HPA, they have been numbered in a consistent scheme. Based on our knowledge, there is not any report of computational studies on the IPT reactions of 6HPA and their dimers, so these calculations will provide a useful interpretation of data in literature 6HPA reaction, theoretically.

COMPUTATIONAL DETAILS AND METHODOLOGY

By following the Isin's method [7] and our recent paper [18] in this paper, we carried out calculations using Becke's Three Parameter Hybrid Functional together with the correlation functional of Lee, Yang, and Parr (B3LYP) methods [31,32] for 6HPA in the gas phase, chloroform, THF, methanol and water in order to evaluate the effect of the solvent on IPT. Also, computations on 6HPA dimers with two different structures were performed in the gas phase at the B3LYP/6-31++G(d) level. All calculations were carried out using the Gaussian 09 suite of programs [33]. The stationary structures (**Enol** and **Keto**) in the IPT reaction of 6HPA and (**2Enol** and **2Keto**) in the dimerization of 6HPA were optimized using density functional theory (DFT) at the most popular B3LYP method [31,34] and a double-ζ basis set with an extra d polarization function and diffuse functions on all atoms (6-31++G(d)).

The vibrational frequencies were obtained at the same level to characterize the local minimum and the Transition states (corresponding to a single negative eigenvalue of the Hessian). The nonspecific solvent effects of the medium were studied by means of the conductor-polarizable continuum model (CPCM) [35]. The CPCM has been used for energy calculations with different dielectric constants (ε = 4.9, $CHCl_3$; ε = 7.42, THF; ε = 32.63, CH_3OH; ε = 78.39, H_2O) in the IPT reactions of 6HPA. The basis set superposition error (BSSE) associated with the hydrogen bond energy in the dimerization of 6HPA was computed *via* the counterpoise method using the individual bases as fragments [36]. The molecular electrostatic potential (ESP) is calculated from the charge density (the continuous electron density and the discrete nuclear charge distribution). ESP maps are very useful three dimensional diagrams of molecules. They enable us to visualize the charge distributions and charge related properties of molecules. They also allow us to visualize the size and shape of molecules. There are no grand equations to describe how complex molecules interact with one another, so the best alternative is to use ESP maps. General chemistry strongly focuses on the charge distributions of molecules. Organic chemistry expands on this molecular property and focuses on reactive sites. Reactive sites are charged regions of a molecule that play a significant role in determining the behavior of other charged molecules in the vicinity. In the majority of the ESP maps, the maximum negative region which is preferred site for electrophilic attack exhibited as red color, while the maximum positive region which is preferred site for nucleophilic attack shown

as blue color [37,38]. ESP maps were calculated for 6HPA dimers.

RESULTS AND DISCUSSION

The B3LYP/6-31++G(d) optimized geometries for **Enol**, **Keto** and **TS** (the transition state) are shown in Fig. 1, and selected structural parameters are listed in Table 1. The IPT reaction **Enol** → **TS** → **Keto** was considered. H-atom transfer from the O14 to the N9 is accompanied by a rearrangement of the six-membered ring, and substantial changes are observed in the carbon-oxygen, nitrogen-hydrogen and oxygen-hydrogen bonds. The distance between H15 and O14 increases during the IPT process. The N9-H15 and O14-H15 distances for **TS** are 1.313 Å and 1.376 Å in the gas phase. Compared to the initial values, it can be concluded that the O14-H15 bond is broken and an N9-H15 bond is formed during the IPT process of 6HPA. During proton transfer in reaction channel **Enol** → **TS** → **Keto**, the C1-C2, C2-C10, C3-O14 and C10-O12 distances

Table 1. Selected Bond Lengths and Angles as Derived from B3LYP/6-31++G(d) Geometric Optimization of 6HPA in the Gas and Solution Phases

Parameters[a]	Gas phase			Chloroform			THF			Methanol			Water		
	Enol	TS	Keto	Enol	TS	Keto	Enol	TS	Keto	Enol	TS	Keto	Enol	TS	Keto
Distance															
C1C2	1.395	1.391	1.369	1.394	1.390	1.369	1.393	1.390	1.369	1.393	1.390	1.369	1.393	1.390	1.369
C3C4	1.407	1.416	1.458	1.408	1.412	1.453	1.408	1.411	1.452	1.408	1.411	1.451	1.408	1.411	1.451
C4C5	1.386	1.385	1.366	1.386	1.387	1.368	1.386	1.387	1.368	1.386	1.387	1.369	1.386	1.387	1.369
C2C10	1.502	1.495	1.486	1.500	1.495	1.487	1.500	1.494	1.487	1.500	1.494	1.488	1.500	1.494	1.488
C3O14	1.354	1.292	1.229	1.356	1.302	1.240	1.356	1.303	1.241	1.356	1.305	1.243	1.356	1.306	1.243
C10O12	1.362	1.356	1.350	1.353	1.348	1.343	1.352	1.347	1.342	1.351	1.345	1.340	1.350	1.345	1.341
N9H15	2.267	1.313	1.018	2.286	1.316	1.018	2.288	1.317	1.018	2.292	1.317	1.018	2.292	1.317	1.018
O14H15	0.975	1.376	2.494	0.975	1.367	2.493	0.975	1.366	2.493	0.975	1.364	2.493	0.975	1.364	2.493
C2N9	1.345	1.346	1.369	1.348	1.347	1.370	1.348	1.348	1.370	1.348	1.348	1.370	1.349	1.348	1.370
C3N9	1.323	1.357	1.405	1.324	1.353	1.395	1.324	1.352	1.394	1.324	1.351	1.392	1.324	1.351	1.392
Bond angle															
N9C3O14	117.68	105.70	120.69	117.93	105.35	120.50	117.96	105.31	120.47	118.00	105.24	120.42	118.00	105.22	120.41
N9C2C10	115.12	116.56	114.44	115.11	116.58	114.42	115.12	116.58	114.41	115.12	116.58	114.40	115.13	116.58	114.40
C10O12H13	106.52	106.93	107.14	107.67	108.07	108.26	107.81	108.21	108.40	108.02	108.42	108.59	108.06	108.45	108.62
C1C2N9	123.04	119.16	120.50	123.10	119.07	120.36	123.10	119.06	120.34	123.11	119.04	120.32	123.11	119.04	120.32
C4C3N9	123.98	120.40	113.22	123.97	120.88	113.72	123.97	120.94	113.78	123.97	121.02	113.87	123.97	121.04	113.88
C4C3O14	118.34	133.90	126.09	118.10	133.77	125.78	118.07	133.76	125.75	118.03	133.74	125.71	118.03	133.74	125.71
C2N9C3	118.06	123.25	125.25	117.92	123.02	125.17	117.90	122.99	125.16	117.87	122.95	125.15	117.87	122.94	125.15
C2C10O12	111.96	112.08	113.28	112.31	112.24	113.22	112.35	112.25	113.20	112.40	112.28	113.18	112.41	112.28	113.18
O11C10O12	122.41	123.27	123.47	122.56	123.60	123.94	122.58	123.64	124.01	122.61	123.71	124.11	122.61	123.72	124.13
C2C10O11	125.63	124.65	123.24	125.14	124.16	122.85	125.08	124.10	122.79	124.99	124.02	122.71	124.98	124.00	122.70
C3N9H15	-	75.42	116.69	-	75.47	117.10	-	75.48	117.16	-	75.48	117.24	-	75.48	117.25

[a]Distances in Å; angles in degrees. For numbering of atoms, see Fig. 1.

decrease, the C3-C4 and C3-N9 distance increase, the C1-H6, C4-H7, C5-H8, and O12-H13 distances remain unchanged in all phases. The C4-C5 bond length and the N9C2C10 and C1C2N9 bond angles decrease in **Enol** → **Keto** transfer, while the C2-N9 bond length and the N9C3O14 and C4C3O14 bond angles increase. The C4C3N9 and C2C10O11 bond angles decrease, while the C2N9C3, C10O12H13, C2C10O12 and O11C10O12 bond angles increase in **Enol** → **TS** → **Keto** transfer in all phases. The total electronic energies of the 6HPA are given in Table 2. Let's see how the calculated relative energy for 6HPA changes. The relative energy, as shown in Fig. 2, was calculated as the total electronic energies differences between **TS**s and the initial forms (**Enol**s). The relative

Table 2. Total Electronic Energies (E, in Hartrees) of the 6HPA Forms in the Gas Phase and Solution at 298.150 K and 1.00000 Atm

6HPA form	$E_{\text{Gas phase}}$	$E_{\text{Chloroform}}$	E_{THF}	E_{Methanol}	E_{Water}
Enol	-512.10893862	-512.11925554	-512.12041840	-512.12203172	-512.12231613
TS	-512.04907087	-512.05933629	-512.06052299	-512.06218079	-512.06247446
Keto	-512.11640756	-512.12850232	-512.12991953	-512.13190652	-512.13225940

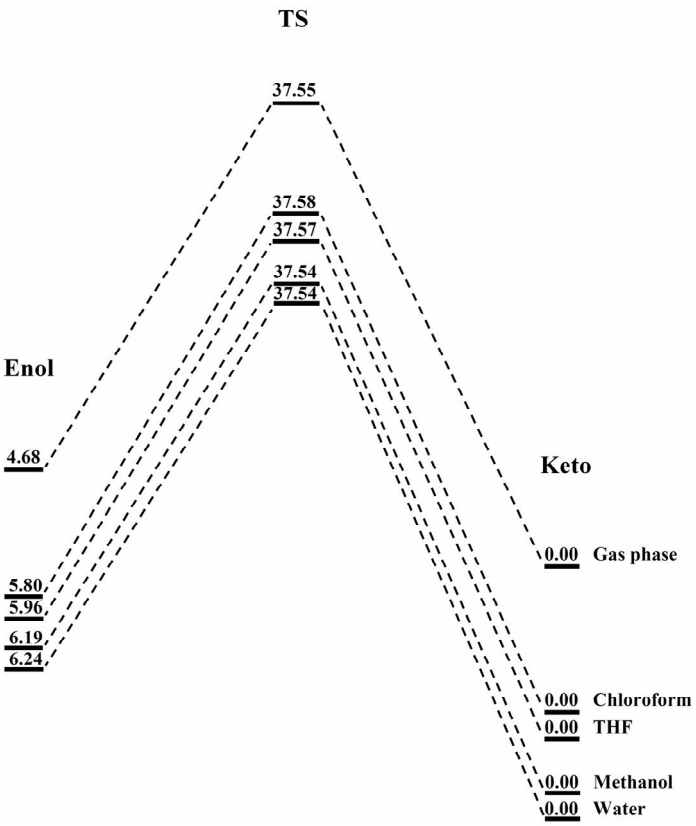

Fig. 2. Energy diagram of the proton transfer process in various solvents (*via* CPCM) and gas phase.

energies of the **TS** with respect to **Enol** were calculated to be 37.55, 37.58, 37.57, 37.54 and 37.54 kcal mol^{-1} in the gas phase, chloroform, THF, methanol, and water, respectively. The barrier height increases on going from the water to the chloroform at the first stage and then decreases on the chloroform to the gas phase. The total electronic energies differences between the two tautomers (**Keto** and **Enol**) were calculated to be -4.68, -5.80, -5.96, -6.19 and -6.24 kcal mol^{-1} in the gas phase, chloroform, THF, methanol, and water, respectively, *i.e.* **Keto** is more stable than **Enol** in the gas phase and solution. As a result, the IPT reaction between **Enol** and **Keto** tautomers occurs almost similarly in the gas phase and solution. Similar two coupled barrier heights were observed for all of the solutions. So, we can conclude that the IPT reaction barrier is decreased with increase in dipole moment of solvent.

From the viewpoint of valence theory, the interaction between the lone pair of the N as acceptor atom and O-H σ* orbitals is mainly responsible for the proton transfer. Therefore, the O-H···N angle and the N···H distance (in **Enol** tautomer) may play an important roles in the proton transfer reactions. In most cases, hydrogen bonds with linear O-H···N structures and short hydrogen bond distances are considered to be strong. In **Enol** tautomer, the O14-H15···N9 angles are 79.11°, 78.29°, 78.20°, 78.08° and 78.05° in the gas phase, chloroform, THF, methanol, and water, respectively. Additionally, the O14-H15···N9 hydrogen bond lengths of **Enol** tautomer are 2.267 Å, 2.286 Å, 2.288 Å, 2.292 Å and 2.292 Å in the gas phase, chloroform, THF, methanol, and water, respectively. It is clear that the power of O14-H15···N9 hydrogen bond is almost similar in all phases. Therefore, it is reasonable to see almost the same barrier IPT reaction in all phases. Let's now examine the calculated relative Gibbs free energies (ΔG) and activation Gibbs free energy barriers ($\Delta G^{\neq}$) for the IPT reaction of 6HPA in the gas phase and solutions. As seen in Table 3, the ΔG for the IPT reaction of 6HPA is the largest in the gas phase. The $\Delta G^{\neq}$ values are increased on going from the water to the chloroform and then decreased from the chloroform to the gas phase. In accordance to ΔG and $\Delta G^{\neq}$ data, this reaction is thermodynamically and kinetically more favorable in solution than that in the gas phase. The calculated values for ΔE_s and ΔG_s shown in Table 4, reveal that **Keto** automer is the most stable

Table 3. Calculated Gibbs Free Energies and Activation Gibbs Free Energy Barriers (in kcal mol^{-1}) for the IPT Reaction of 6HPA

	ΔG	$\Delta G^{\#}$
Gas phase	-4.28	34.37
Chloroform	-5.26	34.44
THF	-5.40	34.43
Methanol	-5.61	34.41
Water	-5.65	34.41

Table 4. Dipole Moments (μ, in debyes), Solvation Energies $\Delta E_s = E_{solv} - E_{gas}$, and Solvation Gibbs Free Energies $\Delta G_s = G_{solv} - G_{gas}$ (in kcal mol^{-1}) of the 6HPA Forms in the Gas Phase and Solution

	Gas phase	Chloroform (ε = 4.9)			THF (ε = 7.42)			Methanol (ε = 32.63)			Water (ε = 78.39)		
	μ	ΔE_s	ΔG_s	μ	ΔE_s	ΔG_s	μ	ΔE_s	ΔG_s	μ	ΔE_s	ΔG_s	μ
Enol	2.95	-6.47	-6.72	3.92	-7.20	-7.48	4.05	-8.21	-8.53	4.24	-8.39	-8.72	4.28
TS	4.72	-6.44	-6.65	6.09	-7.18	-7.42	6.28	-8.22	-8.49	6.54	-8.41	-8.68	6.59
Keto	5.34	-7.59	-7.70	6.93	-8.48	-8.60	7.14	-9.72	-9.86	7.45	-9.94	-10.08	7.51

structure, presumably due to solvent effects. In addition, solvent effects show that the **TS** structure in solution is more stable than in the gas phase. Consequently, the energy barrier to IPT reaction decreases in solution. Although two 6HPA molecules can bind through two intermolecular hydrogen bonds by using the carboxylate and keto-enol groups, realistically, there are two N-H···O strong intermolecular hydrogen bonds between the two **Keto** molecules [20,22] and O-H···N between the two **Enol** molecules around inversion centers, forming **2Keto** and **2Enol** dimer, respectively. The structural parameters of the tautomer dimer structures calculated at the quantum level are shown in Fig. 3. The optimized geometrical parameters indicate that two tautomers (**Enol** and **Keto**) are fully planar, which is in agreement with the experimental values.

The planarity of these structures is attributed to the strong intermolecular hydrogen bonding and the corresponding ring structure of the 6HPA [20,22]. These two hydrogen bonds in the tautomer dimer structures are equivalent to each other, although **2Keto** is linked in a planar fashion by hydrogen bonds to form a sheet which is contest to **2Enol**. Comparing the monomer and dimer structures in the gas phase reveals that the intermolecular hydrogen bonds affect the molecular structure of the monomer. As seen in Fig. 3, the bond angles and bond lengths of the hydrogen donor (O-H or N-H) and hydrogen acceptor groups (N or C=O) of the **2Enol** and **2Keto** structures differ from the corresponding monomers. For example; the C3O14H15 and N9C3O14 bond angles are increased by 5.62° and 2.37 ° in **2Enol**, respectively. The

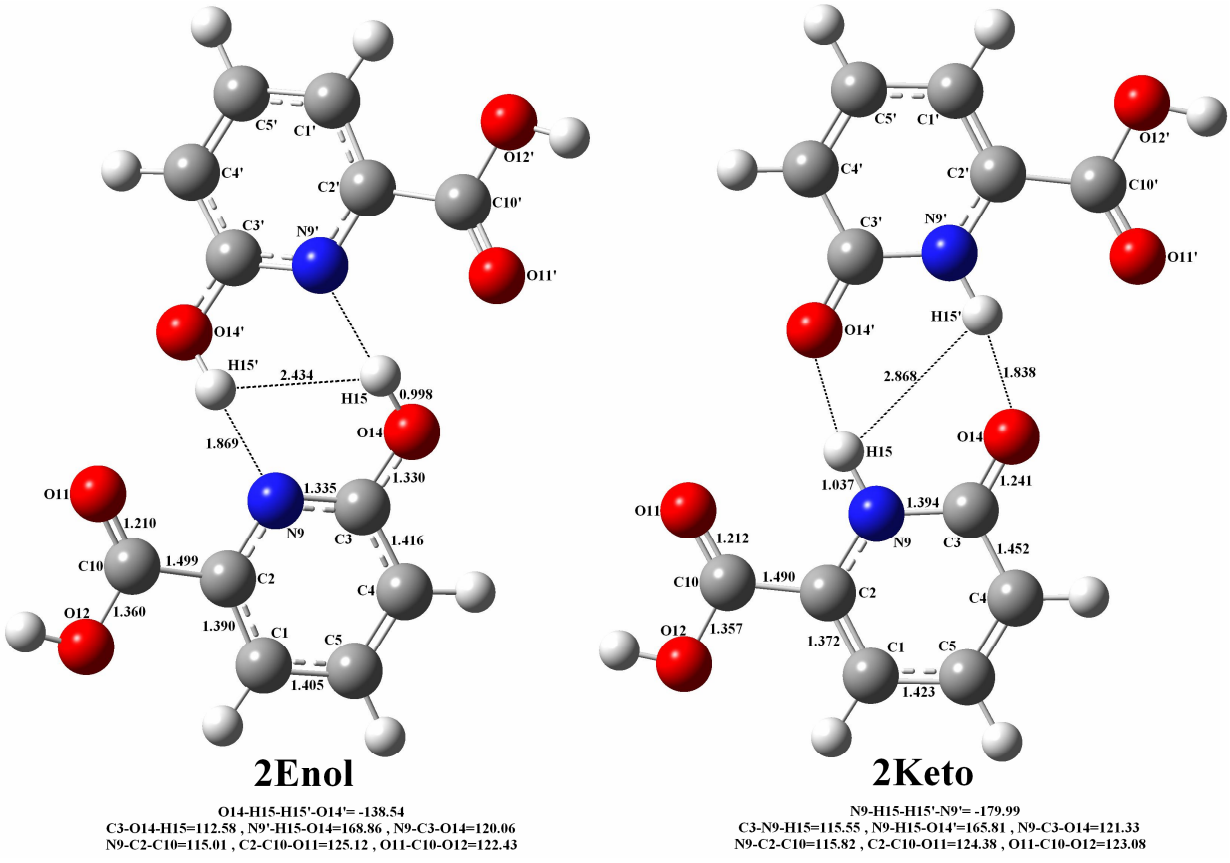

Fig. 3. Optimized tautomer dimer structures of the **2Enol** and **2Keto**. Bond lengths are shown in Å and angles in degrees.

C3N9H15 angle is decreased by 1.14°, while the N9C3O14 angle is increased by 0.64° in **2Keto**. Another important point is the changes in the C3-O14, C3-N9, N9-H15 and O14-H15 bond lengths on going from the monomers to the dimer structures. The results obtained for the gas phase show that the O14-H15 and N9-H15 bond lengths are 0.023 Å and 0.019 Å longer in **2Enol** and **2Keto**, respectively. The C3-O14 bond length is 0.024 Å shorter in **2Enol**, while it is 0.012 Å longer in **2Keto**. The C3-N9 bond length is 0.012 Å longer in **2Enol**, while it is 0.011 Å shorter in **2Keto**. The O11C10O12 bond angle is increased by 0.02° in **2Enol**, while it is decreased by 0.39° in **2Keto**. The C2C10O11 bond angle is decreased by 0.51° in **2Enol**, while it is increased by 1.14° in **2Keto**. Additionally, there are changes in the spatial positions on going from the monomers to the dimeric structures. The O14H15H15'O14' and N9H15H15'N9' angles are -138.54° and -179.99° in **2Enol** and **2Keto**, respectively. The O14-H15···N9' hydrogen bond length and the O14-H15···N9' angle are 0.031 Å longer and 3.05° wider than same values for N9-H15···O14' hydrogen bond in **2Enol** and **2Keto**, respectively. The values of the calculated uncorrected hydrogen-bonding interaction energies, E_{int} and the corrected interaction energies, $E_{cp\text{-}int}$ are given in Table 5. The interaction energies are corrected for basis set superposition error (BSSE) at the B3LYP level using an

Table 5. Calculated Interaction Energies E_{int}, BSSEs, Corrected Interaction Energies $E_{cp\text{-}int}$ and Gibbs Free Energies ΔG (all in kcal mol^{-1}) for the Dimerization of the 6HPA Frorms, in the Gas Phase

Dimer	E_{int}	BSSE	$E_{cp\text{-}int}$	ΔG
2Enol	-13.95	1.66	-12.29	-1.57
2Keto	-19.16	1.07	-18.09	-7.22

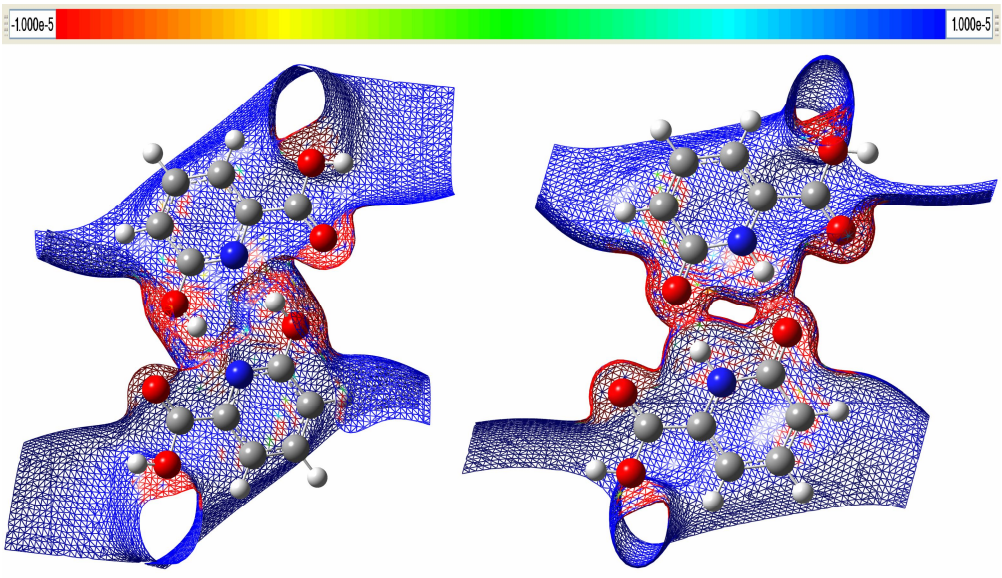

2Enol **2Keto**

Fig. 4. Electrostatic potential maps for tautomer dimer structures (for interpretation of the references to color in the text, the reader is referred to the web version of this article).

approximation to the Boys-Bernardi counterpoise method [35], as described below. The E_{int} of the tautomer dimer (for example **2Enol**) is defined as $E_{int} = E_{2Enol} - 2E_{Enol}$, where E_{2Enol} refers to the total electronic energy of the **2Enol**, and E_{Enol} is the total electronic energy of **Enol** tautomer. When the BSSE is taken into account, the $E_{cp\text{-}int}$ is then calculated as $E_{cp\text{-}int} = E_{2Enol} - 2E_{Enol(2Enol)}$, BSSE = $E_{int} - E_{cp\text{-}int}$ where $E_{Enol(2Enol)}$ is the total electronic energy of monomer **Enol** obtained with the extra ghost Gaussian functions placed at the positions of monomer **Enol** in the **2Enol**. As seen from these calculated interaction energies, **2Enol** and **2Keto** are stable. The calculated ΔG values in Table 5, show that **2Keto** is more stable than **2Enol** by 5.65 kcal mol^{-1}. It is interesting that the intermolecular hydrogen bond lengths in **2Keto** are shorter than those for **2Enol**. Therefore the decreased intermolecular hydrogen bonds (by 0.031 Å) in **2Keto** are responsible for this stability. The stabilities of the tautomer dimer structures under investigation can explain the importance of the intermolecular hydrogen bonds of the tautomer dimmers, too. In the present study, 3D plots of ESP maps of 6HPA dimers have been drawn in Fig. 4. Different values of the electrostatic potential at the surface are represented by different colors. Potential increases in the order of red < orange < yellow < green < blue. The color code of these maps is in the range between -0.00001 a.u. (deepest red) and 0.00001 a.u. (deepest blue) in compounds. Blue shows the positively valued surfaces or the relative absence of electrons, whereas red shows the negatively valued surfaces or the relative abundance of electrons. Comparison of the ESP maps of dimers in the gas phase, indicates that intermolecular hydrogen bonds affect the reactive sites. It is apparent from the figure that most of the red regions are concentrated around the intermolecular hydrogen bonds, while most of the blue regions are concentrated around the rings of tautomer dimer structures. This clearly explains that the N-H···O intermolecular hydrogen bonds emerge in the region where electron density is enhanced. This leads to the strengthening of these bonds. These results confirm that intermolecular hydrogen bonds in **2Keto** are stronger than those in **2Enol** since the higher negative charge density has been used to form them.

CONCLUSIONS

Our computational study suggests that the **keto** tautomer is more stable than **Enol** tautomer in the gas phase and solution. The barrier height for the proton transfer reaction of 6HPA first increases upon shifting from the water to the chloroform and then decreases on going from the chloroform to the gas phase. As a result, the intramolecular proton transfer reaction between **Enol** and **Keto** tautomers is thermodynamically and kinetically easier in solution than that in the gas phase. On the other hand, the geometrical parameters of the two monomer molecules in the **2Keto** and **2Enol** structures are different. Dimerizations of two tautomers (**Enol** and **Keto**) occur spontaneously, while **2Keto** is more favorable than **2Enol**. That is, the intermolecular hydrogen bonds in the **2Keto** structure are stronger than those in the **2Enol** structure. The results show that the stabilities of the tautomer dimers structures are directly affected by the hydrogen bond lengths and electrostatic potential value in the dimers.

ACKNOWLEDGMENTS

We are grateful to Ferdowsi University of Mashhad (Iran) for financial support of this work (Grant No. 18071/3-2011/10/04).

REFERENCES

[1] M. Mirzaei, H. Aghabozorg, H. Eshtiagh-Hosseini, J. Iran. Chem. Soc. 8 (2011) 580.
[2] V.B. Delchev, H. Mikosch, J. Mol. Model. 13 (2007) 19.
[3] H. Aghabozorg, F. Manteghi, S. Sheshmani, J. Iran. Chem. Soc. 5 (2008) 184.
[4] R.D. Massaro, Y. Dai, E. Blaisten-Barojas, J. Phys. Chem. A113 (2009) 10385.
[5] N. Tezer, N. Karakus, J. Mol. Model. 15 (2009) 223.
[6] S. Ash, S.P. De, S. Pyne, A. Misra, J. Mol. Model. 16 (2010) 831.
[7] D.Ö. Isin, N. Karakus, J. Mol. Model. 16 (2010) 1877.
[8] B.D. Vassil, J. Mol. Model. 16 (2010) 749.
[9] M.J. Tenorio, M.C. Puerta, P. Valerga, S. Moncho, G. Ujaque, A. Lledós, Inorg. Chem. 49 (2010) 6035.
[10] R.D. Massaro, Y. Dai, E. Blaisten-Barojas, J. Chem. Phys. 135 (2011) 164306.
[11] P. Borowski, R. Gawinecki, A. Miłaczewska, A. Skotnicka, K. Woliński, A. Brzyska, J. Mol. Model. 17

(2011) 857.
[12] I. Majerz, M.J. Gutmann, RSC Advances 1 (2011) 219.
[13] V. Enchev, S. Angelova, M. Rogojerov, V. Monev, I. Wawer, M. Tkaczyk, K. Kostova, J. Phys. Chem. A 115 (2011) 2026.
[14] B.J. Ośmiałowski, J. Mol. Model. 18 (2012) 1633.
[15] S.H. Kazemi, H. Eshtiagh-Hosseini, M. Mirzaei, 9th Iranian Seminar on Organic Chemistry, Rafsanjan, Iran, 5-7 September, Abstract Book (2012) 118.
[16] S.H. Kazemi, H. Eshtiagh-Hosseini, M. Mirzaei, 9th Iranian Seminar on Organic Chemistry, Rafsanjan, Iran, 5-7 September, Abstract Book (2012) 119.
[17] P. Halder, S. Taraphder, J. Mol. Model. 19 (2013) 289.
[18] S.H. Kazemi, H. Eshtiagh-Hosseini, M. Mirzaei, Comput. Theor. Chem. 1004 (2013) 69.
[19] S. Badoğlu, Ş. Yurdakul, Spectrochim. Acta. 101A (2013) 14.
[20] K. Sawada, Y. Ohashi, Acta Cryst. C54 (1998) 1491.
[21] C.Y. Sun, X.J. Zheng, L.P. Jin, Z. Anorg. Allg. Chem. 630 (2004) 1342.
[22] B.M. Kukovec, Z. Popović, G. Pavlović, M. Rajić Linarić, J. Mol. Struct. 882 (2008) 47.
[23] G.Q. Bian, T. Kuroda-Sowa, H. Konaka, M. Maekawa, M. Munakatza, Acta Cryst. C 60 (2004) m338.
[24] A. Şengül, O. Büyükgüngör, Acta Cryst. C61 (2005) m119.
[25] B.M. Kukovec, Z. Popović, G. Pavlović, Acta Chim. Slov. 55 (2008) 779.
[26] B.M. Kukovec, P.D. Vaz, Z. Popović, M.J. Calhorda, K. Furić, G. Pavlović, M. Rajić Linarić, Cryst. Growth Des. 8 (2008) 3465.
[27] C.Y. Sun, J. Zhou, W.J. Li, L.P. Jin, Z. Anorg. Allg. Chem. 634 (2008) 549.
[28] S.K. Kang, Y.S. Shim, Acta Cryst. E67 (2011) m1237.
[29] B.M. Kukovec, M. Kakša, Z. Popović, Croat. Chem. Acta 85 (2012) 479.
[30] M. Hemamalini, H.K. Fun, E66 (2010) o2246.
[31] C. Lee, W. Yang, P.G. Parr, Phys. Rev. B 37 (1988) 785.
[32] A.D. Becke, J. Chem. Phys. 98 (1993) 5648.
[33] M.J. Frisch, G.W. Trucks, H.B. Schlegel, *et al.*, GAUSSIAN 09, Gaussian, Inc., Wallingford, CT, 2009.
[34] A.D. Becke, Phys. Rev. A38 (1988) 3098.
[35] V. Barone, M. Cossi, J. Phys. Chem. A 102 (1998) 1995.
[36] S.F. Boys, F. Bernardi, Mol. Phys. 19 (1970) 553.
[37] N.R. Dhumal, Spectrochim. Acta. 79A (2011) 654.
[38] M. Karabacak, E. Kose, A. Atac, Spectrochim. Acta. 91A (2012) 83.